Role of the implosion kinetic energy in determining the kilovolt x-ray emission from aluminum-wire-array implosions

C. Deeney, T. Nash, R. R. Prasad, and L. Warren
Physics International Company, 2700 Merced Street, San Leandro, California 94577

K. G. Whitney, J. W. Thornhill, and M. C. Coulter*
Naval Research Laboratory, 4555 Overlook Avenue SW, Washington, D.C. 20375
(Received 6 June 1991)

Aluminium wire arrays have been imploded on the 6-TW, 4-MA Double-EAGLE generator. An initial diameter of 12.5 mm and mass loading of 164 μg/cm have been identified as the optimum parameters to maximize the aluminum kilovolt K-shell yield. The implosion time of 90 ns and the initial radius of 0.625 cm correspond to an implosion kinetic energy of 19.2±3.6 keV/ion. Larger-diameter arrays have higher kinetic energies per ion but lower masses, and they produce lower kilovolt K-shell x-ray yields. Smaller-diameter arrays have kinetic energies per ion less than the minimum 12 keV required to ionize aluminum to its K shell; so these arrays produce lower K-shell yields. Time-resolved x-ray pinhole photography and time-resolved spectroscopy are utilized to determine the K-shell emitting plasmas' sizes, temperatures, and densities as functions of time during the pinched phase. It is found that both the percentage of the mass radiating K-shell x rays and the electron temperature increase during the first 20 ns of emission. For the optimum implosion parameters, it is found that only a small percentage of the mass is radiating in the K shell and, furthermore, that the conversion of kinetic energy to kilovolt emissions alone does not account for the measured x-ray yields. The data analysis suggests that the problem of maximizing aluminum K-shell emission breaks down into two parts. On the one hand, K-shell emission is enhanced when, during the implosion phase, sufficient kinetic energy is generated to drive the aluminum plasma into the K shell on thermalization. This is in agreement with pure-kinetic-energy calculations. On the other hand, there appears to be an additional anomalous heating mechanism that scales with mass and adds to the K-shell emission during the current confinement on axis. As a result, the optimum x-ray production occurs in these experiments by maximizing the mass on axis while both achieving enough kinetic energy per ion and imploding at peak current.

PACS number(s): 52.25.Nr, 52.65.+z, 52.50.−b, 52.25.−b

I. INTRODUCTION

In this paper we describe experiments that examine some of the basic principles of radiation production in imploding wire-array Z pinches, especially the role of the implosion kinetic energy in determining the kilovolt x-ray yield. The experiments involve systematically varying the wire-array parameters, while at the same time measuring the final plasma sizes, densities, and temperatures, as well as the radiated yields. Furthermore, we compare these results with some detailed numerical calculations based on the same initial conditions. This work extends further and in more detail previous experiments and theories on Z-pinch radiation physics, which we now review.

In 1976, Stallings, Nielsen, and Schneider [1] reported that a wire array was better coupled to a 1-Ω waterline pulsed power generator than a single on-axis wire. These experiments found that due to the high initial inductance (40–60 nH) of single wires, only 40% of the generator current flowed in them at the time of peak current. On the other hand, all the current was found to flow through wire arrays which had lower inductances. Kilovolt x-ray measurements of wire arrays [3,4] (and gas puffs [5]) have shown these Z pinches to be very efficient radiators and this was and still is the main motivation for their study.

There are also differences in the way the wire arrays are heated. An array is accelerated to the axis by the interaction of the electrical current and the self-generated magnetic field. During this radial collapse, the moving plasma gains kinetic energy, which is then thermalized by the assembly on axis. In contrast, the single wire is heated by the current from the start of the pulse and it does not benefit from an implosion stage.

One of the assumptions often used to describe the radial dynamics of an array implosion is that all of the current flows through and acts on all the wire mass. The resulting $\mathbf{J}\times\mathbf{B}$ force accelerates this mass, increasing its kinetic energy as it implodes to the axis. Optimum kinetic-energy generation occurs when the array reaches the axis near the time that the short-circuit current peaks. Under the above force assumption, it is sufficient to describe the implosion by the following dimensionless, nonhydrodymamic, equation of motion, as first discussed by Katzenstein [2]

$$\frac{d^2x}{d\tau^2} = -A\frac{i^2}{x}\ , \tag{1}$$

where A is a dimensionless parameter that can be defined in terms of the plasma implosion time t_0, the initial array mass per unit length m, the peak current I_0, the initial array radius r_0, and the number of wires N. The parameters τ, i, and x are the normalized time, current, and radial position, as in Ref. [2]. Specifically, A is defined as

$$A=\frac{N}{N-1}\frac{\mu_0}{4\pi}\frac{I_0^2}{m(r_0/t_0)^2} . \quad (2)$$

Equation (1) can be incorporated with a circuit model for the generator and then solved numerically to predict the plasma radius as a function of time. Comparisons with optical streak camera images [6] show such predictions to be accurate. Equation (1) can also be solved analytically if a current wave form and implosion radius are assumed. The analytical solutions are typically assumed to be valid up to the point where the shell mass is collapsed to 10% of its initial radius [2]. These solutions have been used (a) to predict the implosion time for a given initial radius and mass [3,4] (b) to estimate the shell's mass from the implosion time and initial radius [7], for an uncharacterized source; (c) to derive a phenomenological explanation of the observed I^4 current scaling of K-shell x-ray yields [8]; (d) to determine the optimum coupling of an imploding load to a pulsed power generator [2,9]; and (e) to help theoretically determine the scaling of Z-pinch x-ray emission with atomic number [10]. In this last work, in an attempt to obtain a better theoretical understanding of aluminum kilovolt yield behavior, Whitney *et al.* [10] reported results from one-dimensional hydrodynamic calculations, incorporating full radiation transport. In these calculations, aluminum arrays were driven by a linearly rising current from a fixed radius of 1 cm. To remain consistent with earlier modeling and, more importantly, to focus on the kinetic-energy contribution to the radiated yield, the current was switched off when the plasma reached 14% of its initial radius. The thin shell was then allowed to collapse onto the axis where it was confined by inertia only. The kilovolt x-ray yields from the aluminum wire arrays were determined for varying masses, currents, implosion times, shell kinetic energies and dimensionless kinetic energies per ion (η). The quantity η, is defined by

$$K_i=\eta E_{\min} , \quad (3)$$

where K_i is the maximum implosion kinetic energy per ion and $E_{\min}$ is the sum of the ionization energies and the ion and electron thermal energies required to reach the heliumlike stage of aluminum (or the relevant element of atomic number Z). The temperature used to calculate the thermal energies is chosen to give high K-shell occupation as discussed in Ref. [10]. A scaling law for $E_{\min}$ is

$$E_{\min}=1.012Z^{3.662}\ \text{eV/ion} . \quad (4)$$

For aluminum $E_{\min}$ is 12 keV/ion, while for nickel $E_{\min}$ is 200 keV/ion. Whitney *et al.* [10] in their calculations showed that the parameter η is important in determining how efficiently the energy in excess of $E_{\min}$ is radiated, once the K shell of aluminum is reached by the thermalization of the implosion kinetic energy. For high-mass cases, the conversion of kinetic energy to radiation approached 35%, where it tended to saturate. This saturation resulted in the transition from I^4 to I^2 current scaling. For low-mass cases, however, higher η values, at a given mass, reduced the conversion efficiency due to the plasma being superheated and the density being reduced. For implosions with $\eta<1$, no significant kilovolt radiation production was expected. Some of these trends have not previously been observed in experiments and it is one of the purposes of our experiments to make detailed comparisons of the trends in the theoretical calculations with actual experiments.

Experiments on a particular pulsed power generator, however, are constrained by a fixed rise time and current magnitude; therefore it is not possible to duplicate all of the theoretical conditions of Ref. [10]. For instance, in order to implode at the time of peak current it is necessary to make mr_0^2 a constant according to Eq. (2). Thus the radius of the array must be changed as the mass is varied to maintain optimum kinetic-energy generation. In this case, the kinetic energy per ion cannot be fixed. It decreases as the mass increases. Consequently, the electron temperatures and densities of the imploded plasmas can be expected to vary more than in calculations where either the mass or the kinetic energy per ion are held fixed.

The importance of these parameters in determining the kilovolt x-ray yield, where mr_0^2 was a constant, has already been demonstrated in part on the Blackjack 5 generator at Maxwell Laboratories (MLI). In the reported experiment [3], Gersten *et al.* measured the variation of the kilovolt x-ray yield with aluminum wire arrays. The initial load masses and radii of the arrays were varied, but the quantity mr_0^2 was kept constant, thereby fixing the implosion time and the machine coupling efficiency. It was observed that the aluminum K-shell yield fell from 20 to 0.45 kJ as the initial wire array diameter was increased from 15 to 30 mm, even though the kinetic energy of the imploding shell was approximately the same, in all cases. The time-integrated K-shell spectra were analyzed to give the plasma electron temperatures, while the K-shell yields and the associated pinhole images allowed the plasma electron densities to be estimated. These data indicated that as the initial radius was increased, the electron temperature also increased but the electron density decreased. A similar trend has been observed by Stephanakis *et al.* [11] in neon-gas puff experiments on the Gamble II generator at the Naval Research Laboratory (NRL). The decreasing densities and masses were responsible, in part, for the decrease in the K-shell yields in both experiments. However, since the 15-mm array only reached a minimum η of 4.2, the MLI aluminum experiments neither determined the radius to produce the maximum K-shell yield nor did they observe the yield behavior near the transition $\eta=1$.

A third radius scaling experiment has been performed with nickel wire arrays [4] on the Double-EAGLE generator at Physics International. These experiments showed that there was an optimum initial diameter which maximized the kilovolt nickel L-shell emission. Arrays

of larger diameter than the optimum 15 mm produce less yield for the same reasons as in the MLI and NRL experiments. Smaller array diameters resulted in bulk plasmas which were too cold to radiate 1-keV radiation, although *hot spots* were formed which did radiate 1-keV radiation but at lower yield levels.

In this paper, we describe a set of imploding aluminum-wire-array experiments performed on the DNA/Double-EAGLE generator at Physics International. The first experiment is designed to vary the η value below 1 and to determine the optimum radius and corresponding η value that maximizes the aluminum K-shell yield. In a second experiment, the array masses are varied, at the optimum radius condition, to determine the effect of changing the masses, implosion times, and η values for a fixed initial diameter. The third and final experiment employs an exploding single wire of a comparable mass per unit length as the optimum array to compare the total and K-shell x-ray yields with and without an implosion phase. By comparing all these yields with each other and with those calculated yields from Ref. [10], it is also possible to evaluate whether all of the radiated yield can be attributed to the thermalization and conversion of the kinetic energy alone or whether other heating mechanisms are contributing to the radiated yield. This is one of the main themes of this paper. Such comparisons are instructive, but a number of important differences between the calculations and the experiments are found by diagnosing the plasma thoroughly.

In these aluminum-wire-array experiments, a comprehensive suite [12] of time-resolved pinhole cameras, time-resolved crystal and grazing incidence spectrometers, and yield diagnostics are applied to study the time dependence of the pinch parameters. As a result, we infer time-resolved densities, temperatures, and K-shell emission masses for a set of different initial radius and η implosions. The temperature and density temporal histories are based on the time-resolved data, which are analyzed following the self-consistent approach developed by Coulter, Whitney, and Thornill [13]. These measured plasma conditions also give pointers to additional radiation production mechanisms in imploding Z pinches when they are compared to kinetic-energy-based calculations of the temperatures, densities, and K-shell radiation emitting masses. These time-resolved measurements and their comparison with calculations are a second theme of the paper.

The paper is structured as follows. In Sec. II, we describe the Double-EAGLE generator and the x-ray diagnostics. The results from the radius scaling experiment are analyzed and compared against other experiments in Sec. III. Calculation-experiment comparisons are made in Sec. IV. In Sec. V, the array results are compared with the single wire results, and an interpretation of the experimental findings will be given. We draw our conclusions in Sec. VI.

II. EXPERIMENTAL ARRANGEMENT

The Double-EAGLE [14] generator is composed of two triplate waterline modules feeding a common vacuum diode. When wire arrays are placed between the anode and the cathode a 3 to 4-MA, 110-ns rise time current pulse is delivered to the load. Figure 1 shows a load current trace and the associated aluminum K-shell x-ray pulse for a 15-mm-diam array. The wire arrays used are preloaded into fixtures which hold them at the selected wire array diameter. All the arrays are composed of twelve 2-cm-long wires. Aluminum is the element of choice since extensive modeling has been performed for aluminum implosions and it is also expected to radiate in the I^2 regime.

A comprehensive suite of x-ray diagnostics [12] is employed to measure the aluminum K- and L-shell x-ray emissions. The total x-ray emission around 1.5–2 keV is determined using 2.5-μm-Kimfol plus 1.8-μm-aluminum filtered, tantalum foil calorimeters. In addition, aluminum cathode, x-ray diodes [15] (XRD's) with identical filters are used to measure the radiation power in the same energy range, following Young, Stephanakis, and Scherrer [16]. The XRD emission power signals were also numerically integrated in time to give the kilovolt K-shell yield. An unfiltered calorimeter measures the total radiated yield.

The spatial and temporal behavior of different photon energy emitting regions are studied using filtered pinhole cameras. The filters were chosen to transmit photons with energies greater than 100 and 1000 eV. Time resolution was incorporated into the pinhole cameras by using gated microchannel plates (MCP). The gating strips have a factor-of-4 demagnified images of the plasma produced on them by 50-μm-diam pinholes. Seven or twelve strips are used per camera and each strip is gated with a 5-ns-long, 1-kV pulse. Moreover, each strip is pulsed 5 ns after the preceding strip; thus 35–60 ns of uninterrupted plasma emission could be studied. The strips derived their gating pulse from a common Krytron pulser, which allows for accurate time correlation.

A space-resolved 5-cm-curved mica ($2d = 19.6$ Å) crystal spectrometer gives spectral information on the aluminum K-shell radiation with a spatial resolution of 800 μm. Additionally, a second mica crystal spectrometer, fitted with a five strip gated MCP, is used to time resolve the Al XII resonance and intercombination lines as well as

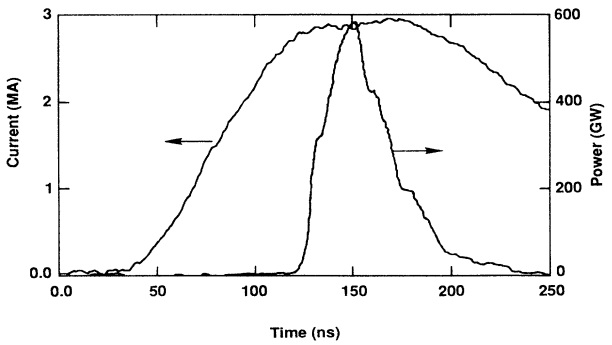

FIG. 1. Load current and the K-shell x-ray pulse for a 0.75-cm initial radius array. The mass loading for this shot is 164 μg/cm and the corresponding implosion time is 85 ns.

the Al XIII $1s$-$2p$ ^1P line, between 7 and 8 Å. The gating pulses for this spectrometer are 10 ns long: twice the length of the pinhole camera pulses.

III. ALUMINUM-WIRE-ARRAY RESULTS

A. Radius scaling

The first part of this experiment involves following the previous prescription for radius scaling experiments. A value of mr_0^2 was chosen to produce implosions at 90 ns. The corresponding mr_0^2 value for the Double-EAGLE generator is 100 μg cm. Due to wire availability in only discrete thicknesses, the actual array mr_0^2 values run from 60 to 120 μg cm and the implosion times vary from 80 to 95 ns. These implosion times are defined as the time from the extrapolated zero of the current rise to the onset of the x-ray emission. Table I lists the actual array parameters tested and the MLI array parameters are also listed in parentheses for comparison. The smaller diameter arrays were chosen to give η less than 1 and hence to observe whether a transition in yield actually occurs at this point.

Figure 2 illustrates the measured kilovolt K-shell yields versus initial radius. At a radius of 0.625 cm, the aluminum K-shell emission is maximized at 35 kJ. The 0.75–1.25-cm radius arrays produce lower yields, with the yield decreasing as the radius increases. The measured yields and the observed behavior agree fairly well with the MLI results, which are also plotted in Fig. 2. Arrays of initial diameter smaller than 0.625 cm are observed to produce hot spots and the emitted K-shell yields decrease markedly. This is identical to previous observations with nickel wire arrays [4]. K-shell-filtered time-resolved images of the pinched plasmas show that the 0.75-cm and large radii array implosions produce plasmas with comparatively uniform K-shell emissions, whereas the 0.3- and 0.45-cm arrays are initially dominated by localized hot spots. However, by some 30 ns after the onset of K-shell x-ray emissions, plasmas appear dominated by instabilities, irrespective of their initial array radius.

A possible interpretation for the transition from hot spot dominated emission to bulk plasma emission that was proposed in Ref. [4] is that the kinetic-energy

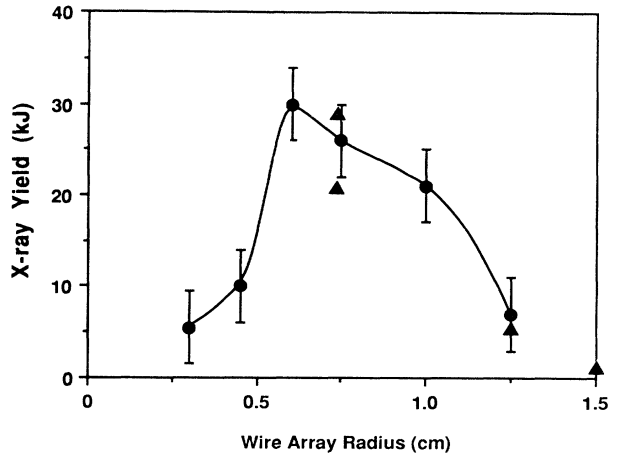

FIG. 2. Measured aluminum K-shell yields (solid circles) vs the initial wire array radius. For comparison, data taken by Gersten *et al.* (Ref. [3]) are shown as solid triangles.

thermalization of the smaller diameter arrays produce plasmas which are too cold to achieve the desired ionization stages (either L-shell or K-shell depending on the element) of the bulk of the plasma. The decrease in temperature is due to the increased mass and decreased implosion velocity. The hot spots are then locally heated either due to instabilities or electron beams. As discussed in Sec. I, this transition is best quantified using the η parameter, which is the ratio of the collapse kinetic energy per ion to the minimum energy required to reach the K-shell (i.e., 12 keV/ion for aluminum). In order to calculate η for these implosions, we estimate the shell kinetic energy by equating it to the work done by the magnetic field on the collapsing shell. The work done is equal to

$$0.5\Delta L I^2 , \tag{5}$$

where ΔL is the change in inductance in going from the array's initial inductance to the final inductance of the pinch and I is the pinch current. The pinch inductance is based on the pinch radius as measured by the softest filtered x-ray pinhole camera. Using this, we calculated the η values tabulated in Table II. Indeed, it is apparent from these calculations that the 0.45-cm implosions had η values less than 1, whereas the 0.625-cm implosion had η of 1.6 ± 0.3. This transition at $\eta=1$ can also be investigated by fixing the initial radius and then varying the ar-

TABLE I. Aluminum radius scaling array parameters. The numbers in parenthesis are those from the Blackjack 5 experiment.

Array radius (cm)	Mass (μg/cm)	mr_0^2 (μg cm)	Implosion time (ns)
0.3	650	59	80
0.45	474	95	90
0.625	277	108	95
0.75	164(130)	93(73)	95(69)
1.0	105(82)	105(82)	95(65)
1.25	80(52)	125(81)	85(64)
1.5	(30)	(67)	(65)

TABLE II. Aluminum radius scaling η values.

Array radius (cm)	η
0.3	0.2
0.45	0.5
0.625	1.6
0.75	1.7
1.0	3
1.25	5

ray mass. In the future, we plan to measure the collapse velocities directly which will give a measure of the η value and then compare the measured η value to those calculated using the technique described above.

B. Mass and implosion time scaling

Logically, therefore, increasing the array mass for a 0.625-cm-diam array should cause both a later implosion and a decreased collapse velocity (kinetic energy per ion) so that η should fall below 1. This would produce a similar effect as the small radii implosions. The results for a 0.625-cm-radius array mass scan are shown in Fig. 3. This shows a plot of the K-shell yield versus the measured implosion time (the mass loadings are listed in Table III). As expected, the more massive array resulted in increased implosion times and $\eta < 1$ (see Table IV). The emission was again dominated by hot spots for $\eta < 1$. Decreasing the array mass to give a 70-ns implosion results in a slightly lower yield from the bulk plasma compared to the 95-ns implosion time. From these data and the radius scaling results, we observe that as η is increased above 1, the K-shell yield decreases. Indeed, the MLI data show similar trends for high η values. This observation is at variance with the modeling in Ref. [10] and it is discussed further in Sec. IV.

Summarizing the experimental data, we observe that $\eta > 1$ for aluminum is achieved by array implosions of initial radius to implosion time ratio greater than 6.25×10^{-3} cm/ns. For η just bigger than 1, the K-shell yield is maximized. Increasing η further by increasing array radius or by decreasing the implosion time results in decreased K-shell yield. If η is less than 1, the K-shell yields are small and the emissions originate from hot spots.

C. Time-integrated spectral data

Although the combination of the radius scan and the mass scan experiments validate the concept of threshold kinetic energy per ion ($\eta > 1$), it is necessary to scrutinize this concept more carefully by analyzing the spectra in these experiments to determine the plasma parameters. This provides further insight into any differences between experiments and the numerical modeling. Time-integrated aluminum K-shell spectra are available for most of the shots taken; an example is shown in Fig. 4. These time-integrated spectra allow analyses similar to those performed by Gersten *et al.*[3] and Burkhalter *et al.* [17] to be carried out. A more complete analysis technique has been proposed by Coulter, Whitney, and Thornhill [13]. This employs a CRE model, with full radiation transport, for the self-consistent-analysis technique. The procedure requires the K-shell emitting radius, the K-shell emitted power (or yield and pulsewidth) per unit length, and the ratio of the Al XIII Ly_α and Al XII He_α lines to be known. By comparing these line ratios as functions of ion density, plasma size, and electron temperature with the power per unit length (or yield per unit length) as functions of the ion density, plasma size, and electron temperature, the plasma opacity is accounted for and the electron temperature and density are determined, self-consistently. Specifically, using the CRE model, isocontours of radiated power per unit lengths and line ratios are plotted versus ion density and electron temperature for a given size of plasma, as determined by the pinhole photographs. For an example of these plots, see Ref. [13]. The intersection of the measured Al XIII Ly_α and Al XII He_α line ratio and the measured power per unit length contours defines the ion density and electron temperature.

Four shots are analyzed: 0.45-, 0.625-, 0.75-, and 1.0-cm-diam arrays. The calculated electron temperatures and ion densities for these four shots are shown in Fig. 5. The ion density is observed to monotonically decrease as the initial array diameter increases (and initial mass loading decreases). On the other hand, the electron temperature is almost constant around 950 eV, for the 0.625–1.0-cm cases and is lower, 600 eV, for the 0.45-cm-radius array. The measured parameters in this experiment appear to agree within a factor of 2 with those reported by Gersten *et al.* We do not observe a clear trend

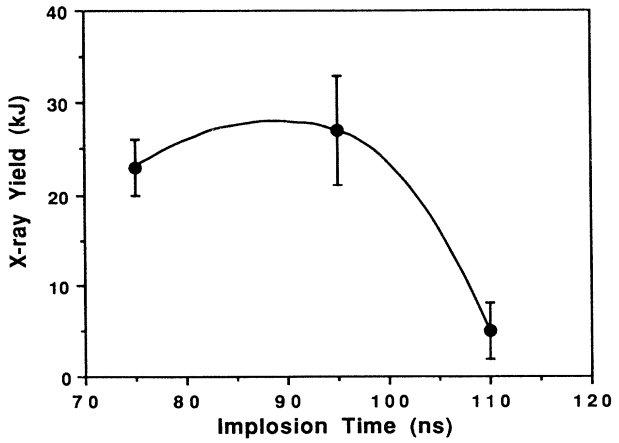

FIG. 3. Measured aluminum K-shell yields vs implosion time for an initial wire array radius of 0.625 cm.

TABLE III. Aluminum mass scaling array parameters.

Array radius (cm)	Mass (μg/cm)	mr_0^2 (μg cm)	Implosion time (ns)
0.625	133	51	70
0.625	277	108	95
0.625	420	164	110

TABLE IV. Aluminum mass scaling η values.

Array radius (cm)	Mass (μg/cm)	η
0.625	133	2.2
0.625	277	1.3
0.625	420	0.9

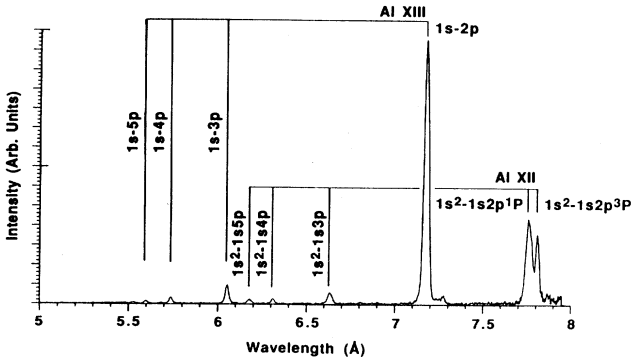

FIG. 4. Time-integrated aluminum spectrum for a 1.0-cm-radius array. The mass loading for this shot is 105 μg/cm and the implosion time is 95 ns.

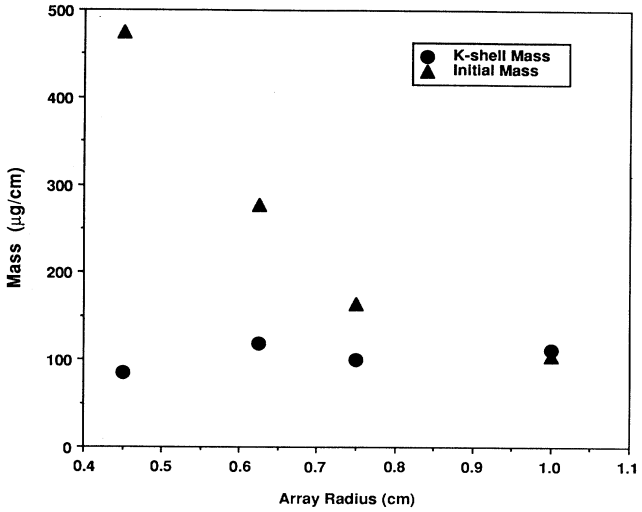

FIG. 6. Comparison of the estimated average K-shell emitting mass with the initial mass loadings of the arrays. In all but the 1.0-cm-radius array, the K-shell mass is significantly less than the initial mass loading.

in the behavior of the electron temperature versus the initial array radius, between 0.625 and 1.0 cm. The density variations, however, appear to follow similar trends as the MLI data. Absolute differences between our data and the MLI data may be due to the different generators, initial mass loadings, and the analysis techniques. Although the ion density for the 0.45-cm-radius array shot is high and the electron temperature is 600 eV, these are the parameters of the hot spots. The actual bulk plasma did not radiate K-shell x-rays as noted from the time-resolved pinhole images. In fact, the mass of plasma radiating K-shell x rays for the 0.45-cm array is 95 μg/cm compared to the initial mass loading of 474 μg/cm, as shown in Fig. 6. The trend in the measured time-integrated K-shell radiating masses (see Fig. 6) does not show any strong variation with initial radius, although the maximum mass is measured for the 0.625-cm shot. Summarizing the time-integrated data, the 0.625-cm shot produces the highest K-shell yield (30 kJ) and it has the highest radiating mass, ion density, and electron temperature. The 0.75 and 1.0-cm shots produce lower yields (28 and 18 kJ, respectively) and they have lower ion densities and K-shell radiating masses. The 0.45-cm shot produces only 12 kJ. Although it has a higher ion density, its electron temperature, K-shell pulse width, and radiating mass are lower than those of the optimum array. Finally, only the 1.0-cm-diam shot has the situation where the K-shell radiating mass equals the initial mass loading.

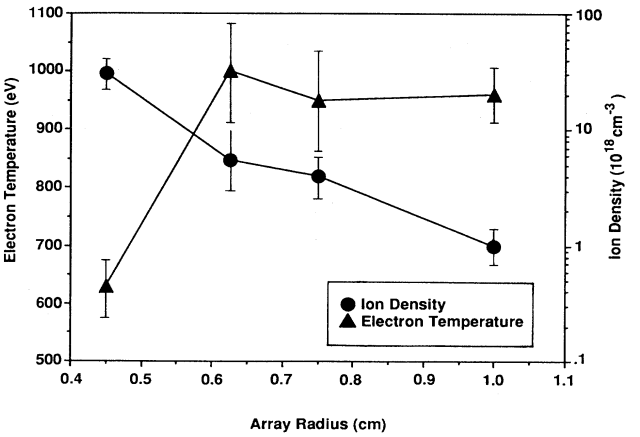

FIG. 5. Average ion densities and electron temperatures vs array radius. As the array radius increases, the ion densities decrease and the electron temperature increases.

D. Time-resolved spectral data

The time-resolve x-ray data also permit a time-resolved analysis of the plasma electron temperatures and densities. Figure 7 illustrates the measured K-shell emitting radius and kilovolt K-shell power for a 0.75-cm-radius array shot. The K-shell powers are measured by the filtered XRD's. The powers displayed in Fig. 7 are determined by calculating the energy emitted in the 10-ns intervals of the crystal spectrometer gates and dividing it by the 10-ns frame time. The K-shell plasma sizes are taken from consecutive time frames of the filtered x-ray pinhole cameras. Figure 8 contains four densitometer scans through the Ly_α and He_α lines for various times during the same shot as in Fig. 7. The spectra are corrected for the film response, crystal reflectivity, and filter transmissions.

An interesting feature in Fig. 7 is that the K-shell emitting power is increasing as the plasma radius is increasing. If one assumes that all the radiated energy is provided by the thermalization of the shell's kinetic energy, then the peak radiated power occurs at the time of the maximum compression of the plasma, i.e., when the plasma is at its minimum radius. There are a few possible explanations for this effect: (i) the imploding shell is actually thick (many mm) as opposed to a thin shell (0.1–1 mm), so that the radiating mass is increasing in time; (ii)

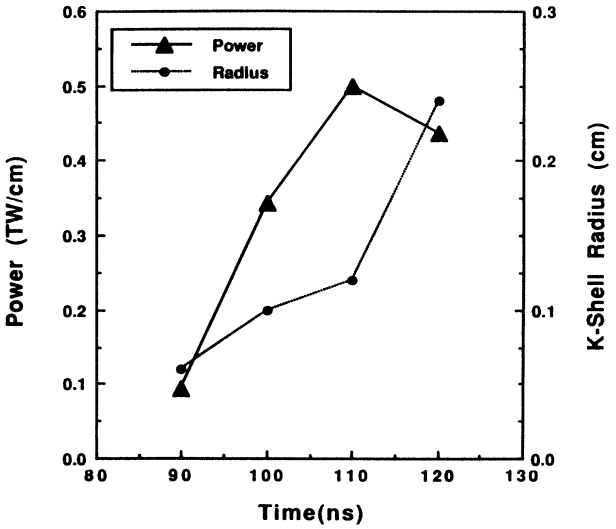

FIG. 7. Temporal evolution of the K-shell radiating power and K-shell plasma radius. The K-shell power increases as the plasma expands. This is for a 0.75-cm-radius, 164-μg/cm shot.

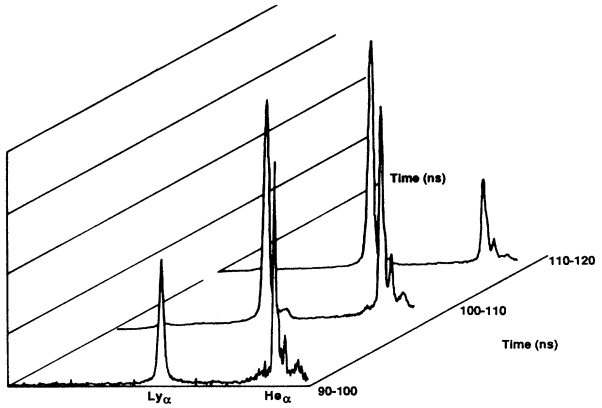

FIG. 8. Densitometer line outs of the K-shell spectra (Ly$_\alpha$ and He$_\alpha$ lines) for three time frames. These spectra are from the same shot as Fig. 7.

all the mass is assembled initially, but the electron temperature in the K-shell radiating mass increases as the plasma expands, and (iii) all the mass assembles initially, then a heating wave propagates slowly into the cool plasma, thus increasing the K-shell radiating mass. Clearly, in Fig. 8, the ratio of the Ly$_\alpha$ to the He$_\alpha$ line increases from less than 1 to greater than 1 in the sequence of time frames. This would indeed indicate that the plasma may be heating while the plasma expands and the radiation power increases.

To quantify this behavior, we have performed a time-resolved-analysis procedure for the same four shots that are analyzed in a time-integrated averaged fashion. All the results are tabulated in Table V. Focusing on the 0.625-, 0.75- and 1.0-cm-radius shots, all three indicate that as the K-shell emitted plasma radius increases, the ion density decreases (or stays constant), and the electron temperature increases (see Fig. 9). The time of peak K-shell x-ray power in all three shots is 120 ns. Another common trend in these shots is that the K-shell radiating masses increases over the first 20–30 ns and then stay constant or fall slightly, as shown in Fig. 10. These confirm that even the peak K-shell emitting masses are significantly less than the initial mass loadings, except for the 1.0-cm-radius arrays.

The mass differences are consistent with the time-resolved pinhole images which show that the plasma radii are larger in the softer filtered (L-shell) pinhole images than in the K-shell filtered images. The differences between the K-shell plasma radii and the sizes of the L-shell filtered images are seen in Fig. 11. The 0.3- and 0.45-cm array shots exhibit the largest difference in plasma radii. The differences are less for the 0.625–1.0-cm-radius arrays. In addition, in all cases, the measured plasma radii

TABLE V. Results of the analysis of the time-resolved spectroscopic data.

Shot	Radius (cm)	Yield (kJ)	Time (ns)	Radius (cm)	He$_\alpha$/Ly$_\alpha$	K-shell power (GW/cm)	T_e (eV)	N_i (10^{19} cm^{-3})	m_k (μg/cm)
2044	0.45	12	110	0.04	0.5	321	640	26.0	59
			120	0.04	0.5	469	660	40.0	90
			130	0.16	0.97	170	720	1.3	47
2029	0.625	30	100	0.02	0.64	44	620	10.0	6
			110	0.06	0.43	250	840	8.5	43
			120	0.10	0.45	469	820	6.4	90
			130	0.28	0.39	375	1300	1.0	110
2045	0.75	28	100	0.05	1.12	156	410	16.0	56
			110	0.10	0.72	344	570	6.9	97
			120	0.12	0.21	500		4.0	81
			130	0.24	0.34	437	1300	1.0	81
2039	1.0	18	110	0.27	0.83	175	980	0.6	64
			120	0.31	0.87	232	960	0.6	84
			130	0.31	0.55	218	1250	0.6	79

are larger than the 10% of the initial array radius often assumed in most calculations to be the minimum radius.

IV. COMPARISON OF ONE-DIMENSIONAL LAMINAR MAGNETOHYDRODYNAMICS CALCULATIONS AND RADIUS SCALING EXPERIMENTAL RESULTS

A. Current-off laminar calculations

In Ref. [10], a yield formula is derived for aluminum array implosions as a function of η and m under the assumption that the kinetic energy generated during the radial collapse is effectively the only energy source for the plasma. This situation, as mentioned earlier, is achieved by terminating the current prior to stagnation. While the current continues to flow in real experiments, it is convenient to turn off a linearly rising current abruptly in the theoretical calculations just before the plasma assembly on axis and the commencement of the kilovolt x-ray emission. When the current is prescribed theoretically in this way, it is possible to accelerate any array mass (m) to any given kinetic energy per ion (η) conveniently in order to calculate unambiguously how this kinetic energy alone is thermalized and converted into x rays. Moreover, a linearly rising current reasonably approximates the rising portion of the experimental current wave forms (see Fig. 1). By carrying out these calculations, one attempts to isolate the yield coming from kinetic-energy conversion from the yield coming from other energy-generating mechanisms that are current driven.

The fluid motion that is calculated when the current is terminated prior to stagnation is shown in Fig. 12, which contains the trajectory of each plasma cell in a typical calculation. The implosion begins at $t=0$ with the array at a radius of 1.25 cm. The linearly rising current is turned off at 85 ns when the outer cell reaches a radius of 0.17 cm. The plasma continues to move inward inertial-

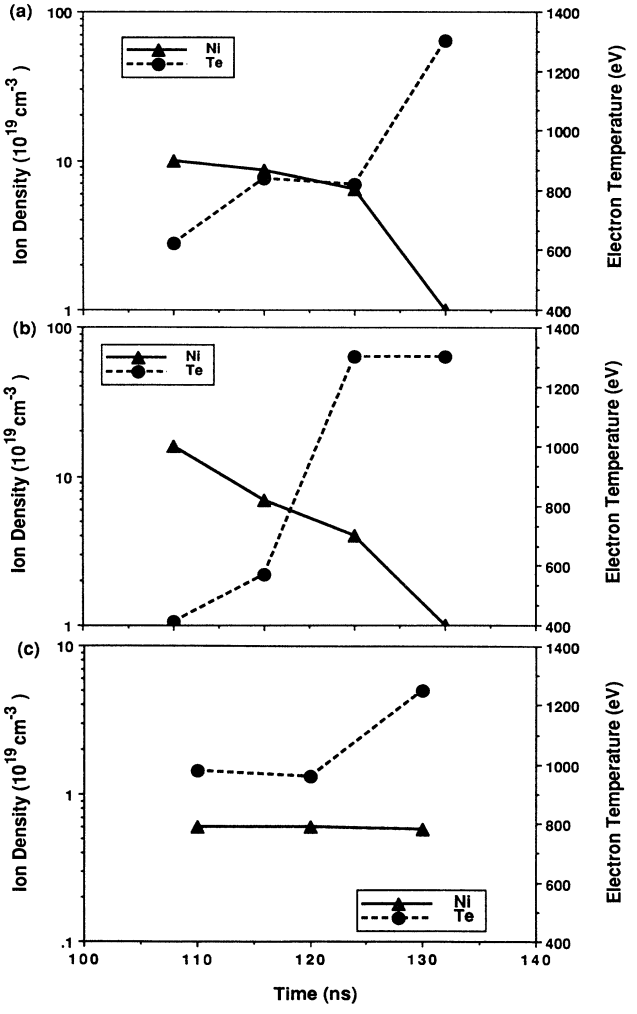

FIG. 9. Measured temporal behavior of the ion densities and electron temperatures for (a) a 0.625-cm array, (b) a 0.75-cm array, and (c) a 1.0-cm array.

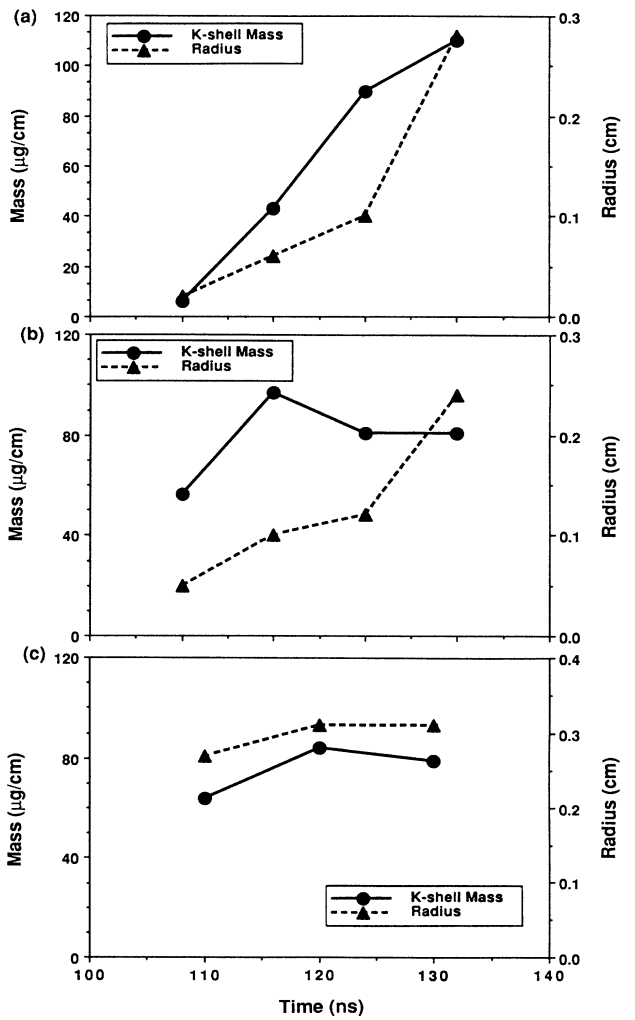

FIG. 10. Measured temporal behavior of the K-shell radiating mass and the K-shell radius for (a) a 0.625-cm array, (b) a 0.75-cm array, and (c) a 1.0-cm array.

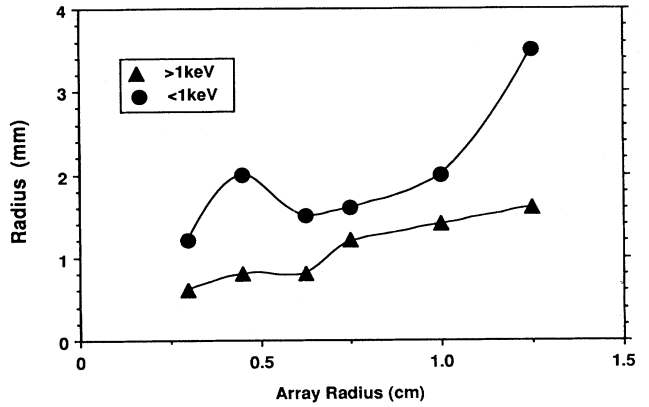

FIG. 11. Comparison of the L-shell (<1 keV) plasma radii and the K-shell (>1 keV) plasma radii as the array initial radius varies. The L-shell radius increase dramatically for the 1.25-cm-radius arrays and for all arrays, the L-shell radii are bigger than the K-shell radii. This is consistent with the K-shell mass being a small fraction of the initial mass (see Fig. 6).

ly. It then stagnates and recoils outward. The total kinetic energy per ion generated by the implosion determines the temperature reached by the plasma (at 88 ns in the example shown), while the mass imploded controls the amount of x radiation emitted during the collision process. Plasma expansion and cooling alone terminate the x-ray emission.

The three basic assumptions of these calculations, are (1) that the flow is nonturbulent, (2) that, during implosion, the $j\times B$ force acts on all of the initial load mass,

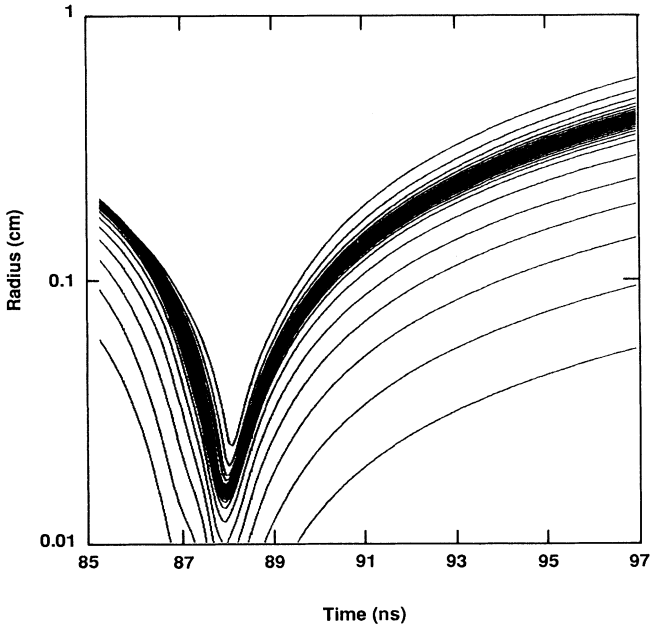

FIG. 12. Example of the trajectories for different zones in the numerical simulations. Notice the tight pinch (<0.03-cm radius) and the short duration of the compression (a few ns).

and (3) that enough kinetic energy per ion is generated during the implosion to drive the plasma well into the K shell, i.e., there is plenty of excess energy available to be radiated. From Ref. [10], the predicted aluminum K-shell yields y_K, as a function of η and m, are

$$y_k(\text{kJ/cm})=\begin{cases} a(\eta)m^2, & m\le m_{BP} \\ b(\eta)m, & m\ge m_{BP} \end{cases} \tag{6}$$

where, for aluminum ($Z=13$),

$$a(\eta)=1.43\times10^{-5}\left[33.7+\frac{595}{\eta}-\frac{70.7}{\eta^2}\right], \tag{7a}$$

$$b(\eta)=1.47\times10^{-2}\eta\ , \tag{7b}$$

and $\eta>1$. Also

$$m_{BP}\ (\mu\text{g/cm})=\frac{b}{a}=1.03\times10^3\eta^3\frac{1}{(33.7\eta^2+595\eta-70.7)}\ . \tag{8}$$

B. Comparison of experimental and calculated yields

Thus for the four experimental cases where $\eta>1$, one can construct a table of predicted yields (see Table VI). If the experimental plasma were to behave as the theoretical predictions, one would conclude that in all cases, the pinches would be radiating in the I^2 (or m) regime; i.e., they would radiate with a 30–35 % conversion efficiency of the kinetic energy into kilovolt x rays, producing the yields shown in the last column of Table VI and plotted as the solid line in Fig. 13. However, the two plasmas are only qualitatively similar. In the current-off calculations, the magnetic forces compressed the plasma during its acceleration, and further compression down to 0.03 cm occurs on axis, in part, because of radiative collapse. During the radiative collapse phase, however, no additional energy is imparted to the pinched plasma since at that time, the current is terminated in the calculation. Consequently, the ideal theoretical plasmas reached high densities on axis and the K-shell radiation pulses are short ($<$ 1 ns). Figure 14 shows a typical power pulse from the calculations. Clearly, these pulses are much shorter than those observed in the experiment (see Fig. 1).

Equally important as the differences in the power pulses, the experimental yields are significantly larger than the theoretical yields calculated in the I^2 regime, on the basis of kinetic-energy conversion alone. This finding provides strong, direct evidence of the existence of a "burn" phase to the x-ray production that is caused by additional heating, especially since the experimental yields peaked near the value of $\eta\ge1$ where the kinetic-energy conversion must be less than 30–40 %. In the experiment, the conversion efficiency is approaching 100%. Possible heating mechanisms will be discussed in Sec. V.

TABLE VI. Aluminum radius scaling parameters based on the scaling law developed in Ref. [12].

Array radius (cm)	m (μg/cm)	η	m_{BP} (μg/cm)	E_{KE} (kJ/cm)	Y_k (kJ/cm)	Y_{tot} (kJ)
0.625	277	1.6	4.4	19.6	6.5	13
0.75	164	1.7	4.9	12.3	4.1	8.2
1.00	105	3	14	14.0	4.6	9.2
1.25	80	5	34	17.7	5.9	11.8

C. Comparison of electron temperatures and ion densities

When four current-off calculations are carried out to accord with the implosion behavior of the four experimental cases in Table VI, the plasmas reached average peak densities that ranged monotonically from 3×10^{22} for the 277-μg/cm, high-mass case to 4×10^{21} for the 80-μg/cm, low-mass case. The corresponding average peak temperatures ranged monotonically from 380 to 970 eV. This decrease in density and increase in temperature with decreasing mass and increasing η agrees qualitatively with the trends in the observed temperatures and densities seen in Fig. 5. However, the experimentally inferred densities of the K-shell emission region are a factor of 100 smaller than the calculated densities.

These observations raise a number of intriguing questions, especially when the results in Figs. 7, 8, 10, and 11 are considered. One-dimensional (1D) magnetohydrodynamics (MHD) calculations appear to agree with experimental findings during the acceleration phase of the implosion, i.e., the implosion times agree. When the experimental array masses are accelerated in the laminar 1D MHD calculations to implode at the observed implosion times, they achieve roughly the kinetic energies that are observed. This finding appears to be confirmed by the fact that the experimental yields dropped markedly and hot spots formed when the kinetic energy per ion fell below the theoretically predicted E_{min} value of 12 keV/ion. At stagnation, on the other hand, the story changes dramatically.

If the experimental implosions had taken place according to the calculations, then by inertia alone, one might expect each implosion to proceed radially inward, as shown in Fig. 12, and to produce a sharp onset to the x-ray pulse (see Fig. 14). Instead, Fig. 1 shows that the kilovolt emission rose slowly from the time of stagnation and peaked roughly 20 ns later. Figures 15 and 16 show the calculated ion density and electron temperature temporal histories. Some zones show rapid increases in electron temperature at thermalization followed by slower falls. In contrast, the other zones have temperatures and densities that fall and rise at approximately the same rate, hence the symmetric radiation pulse (see Fig. 14). Although the calculations exhibit shorter duration events than the experiments, some zones appear to have the same qualitative behavior as the actual experimental density and temperature plots, i.e., we observe a fast increase in electron temperature to around 500 eV or so followed by a slow increase to above 1 keV. The measured ion

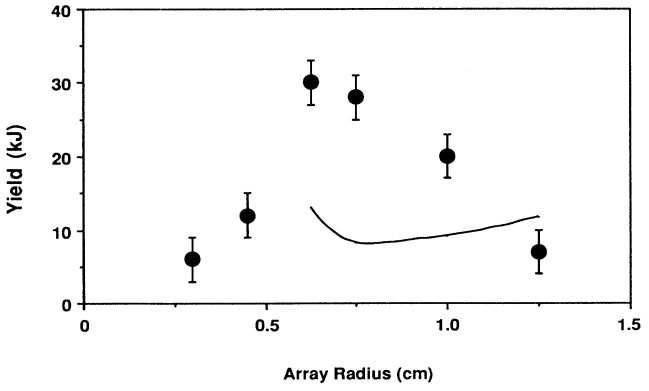

FIG. 13. Measured K-shell yields and the calculated K-shell yields (solid line) vs initial array radius. The simulations predict no radiated K-shell yield below the 0.625-cm arrays. Clearly for the 0.625-cm through 1.0 cm-radii arrays, the measured yields are greater than the predicted yields. Moreover, the trend in the yield behavior is different also.

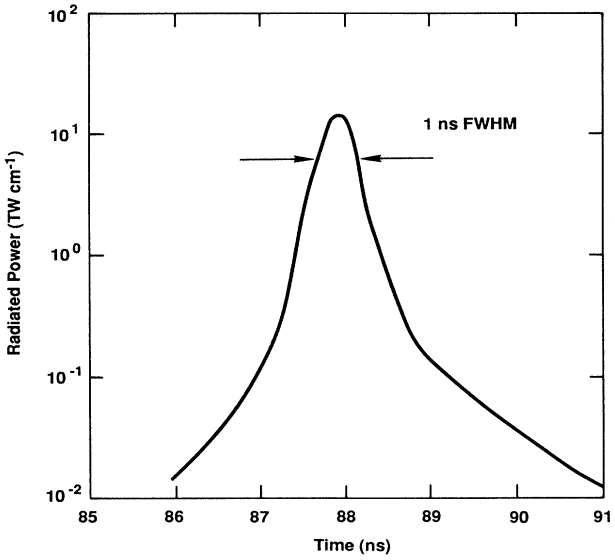

FIG. 14. Typical example of the K-shell radiation pulse calculated by the simulations.

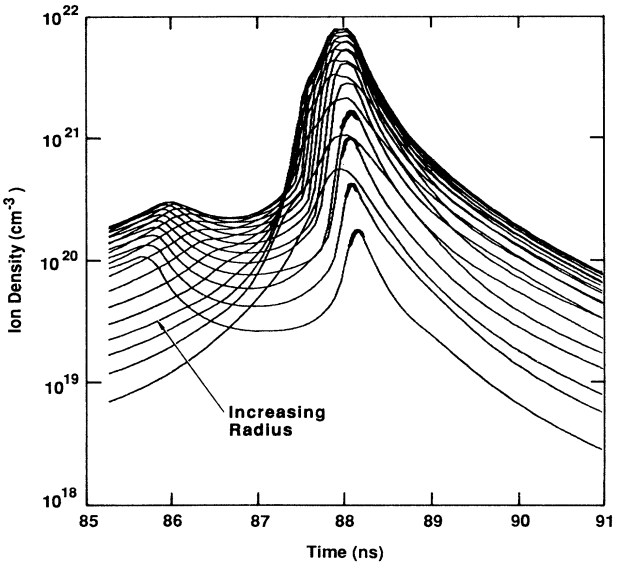

FIG. 15. Ion density trajectories for different zones in the numerical calculations.

density profiles all exhibit a rapid increase followed by a gradual reduction in density. Barring the presence of a hidden mass caused by gradients within the K-shell emission region, which would be unseen in the pinhole picture because of the optical depth of the plasma, the emission of the plasma is seen to grow because the number of emitters grows (Fig. 12) even as their average density falls (Fig. 9). Nevertheless, only a small fraction of the original wire mass ($\sim 30\%$) participates in the K-shell emission in the high yield 277-μg/cm shot (see Fig. 6). The amount of aluminum that radiate in the K shell in all of these experiments seems surprisingly fixed around 100 μg/cm regardless of the mass imploded, equaling the imploded mass only for the 105-μg/cm shot.

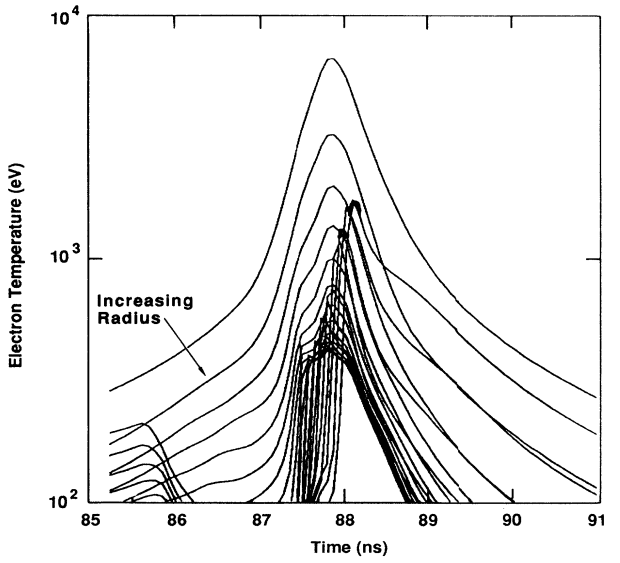

FIG. 16. Electron temperature trajectories for different zones in the numerical calculations.

To summarize, in the aluminum experiments, the plasmas were much less compressed and they emitted over a much longer time than in the current-off calculations; that is, the experimentally produced plasmas are current confined rather than inertially confined. Nevertheless, the experimental yield drops precipitously and hot spots become the source of the radiation when η became less than 1. This finding provides strong evidence for a Z-pinch "ignition" concept, i.e., for the idea that the thermalization of kinetic energy is an important initiating process that is needed to drive the plasma into the correct ionization stages for subsequent efficient x-ray production.

One is still left with explaining the obvious differences between the experiments and the theoretical predictions. First, in the calculations, the 30–40 % conversion efficiencies are achieved with essentially 100% of the initial mass radiating in the K shell, for the 0.625- through 1.25-cm-diam arrays. Although the experiments and calculations agreed in the η values, the experimental K-shell radiating masses are generally less than the initial mass loadings. One could possibly argue that some mass is being left behind during the wire explosion process, as is observed by Riordan *et al.* [8] when very thick wires were utilized on a 1-MA generator. In that case, one would expect the implosion to move earlier in time, if all the current flowed through the smaller imploded mass. A possible explanation, if the implosion time is not different, is that not all the current flows through the reduced mass, i.e., the combination of reduced mass and reduced current gives the same implosion time as if all the current had flowed through all the initial mass. An indication that the initial conditions for an actual wire array may be significantly different from the uniformly filled cylinder assumed by the 1D laminar calculations comes from comparing the nickel results presented in Ref. [4] with the aluminum-wire-array data. Data analysis of the nickel-wire-array implosions indicated that just less than 100% of the initial mass was observed to radiate in the L shell for 0.75-cm-radii wire arrays. The estimated cold skin depth of the nickel for a 100-ns rise-time current pulse is approximately 100 μm. This skin depth is larger than the wire thickness (20 μm). In the aluminum wire arrays, the skin depth is 25 μm, but the wire thicknesses are 20–30 μm. It is not surprising that the initial wire array conditions may effect the quality of the pinch. Indeed, on the SATURN generator increasing the number of wires in array while decreasing the wire thicknesses improved the quality (tightness) of the pinch. Barring this effect, the thermalization of the imploding shell may be different than predicted by the laminar calculations. Future experiments and calculations should aim to resolve this issue. Effects such as 2D flows in the r-z and r-ϑ planes should be investigated. Morever, anomalous resistivity, anomalous viscosity, and a treatment of turbulence may be needed to bring the 1D laminar calculations into better agreement with the experiments.

V. COMPARISON WITH SINGLE WIRE EXPERIMENTS AND INTERPRETATION OF THE DATA

We have determined, in Sec. IV, that the radiated K-shell x-ray yield from 0.625- to 1.0-cm-radius implosions are generally higher than the estimated yields based purely on ideal kinetic-energy thermalization. This has been interpreted as the result of additional heating mechanisms. Enhanced Ohmic heating has previously been proposed [22]. The experiments, however, did indicate that the thermalization of the kinetic energy appeared to promote K-shell ionization. Specifically, when η is less than 1, only hot spots produced K-shell x rays.

In the radius and mass scaling experiments, the initial mass is increased so that η is correspondingly decreased below 1. Hence, if, additional heating occurs it is shared by more mass, thus the plasma will still be cold. To complete the experimental picture therefore, we perform a single-wire experiment. Obviously, as discussed in the Introduction, there is no significant radial collapse phase and hence no significant kinetic-energy input to the plasma; rather, the plasma is primarily Ohmically heated. Before proceeding, there is one caveat to this assumption; it is possible that initially some fraction of the initial mass is blown off and then expands out to a large radius. This low-density blowoff plasma may then implode back onto the wire as the current increases. We have no direct evidence to prove or disprove this hypothesis, so based on the fact that the final plasma radius (hence inductance) is less than that of the initial wire, we will assume that there is no compressional work done on the plasma. If the final plasma state is basically in a Bennett equilibrium (we will discuss the validity of this assumption later in the text), then the plasma electron temperature T_e in eV is determined via the relation

$$T_e = 3.12\times 10^9 \frac{I^2}{(Z+1)N_i} \; ; \tag{9}$$

hence the electron temperature, for a given current (I in amperes), is set by the ion line density (N_i) in units of cm^{-1}. We, therefore, select the mass per unit length of the wire to be 218 μg/cm, which lies between the masses of the 0.625- and 0.75-cm arrays. Both of these arrays achieved significant K-shell ionization, hence, from a Bennett equilibrium argument, so should the single wire. However, η would be effectively zero.

The measured K-shell x-ray yield from the single wire is 4 kJ, which indeed is comparable with the massive, small-diameter arrays. Hot spots were again responsible for these emissions. The kilovolt x-ray emission starts some 80 ns into the current pulse at a current of 2 MA. A peak value of 2.5 MA is reached at 110 ns. The x-ray signature (see Fig. 17) is again consistent with the presence of hot spots. Such hot spots have been observed in previous single-wire experiments [19–21]. The reduction in the peak current is due to the fact that the single wire is much more inductive than the wire arrays. Consequently, a direct comparison based on the Bennett relationship between the single wire and the array must be tempered with the fact that the Bennett temperature for a single-wire plasma is 325 eV, whereas it is between 500 and 750 eV for the two arrays. In addition, the Ohmic heating may be reduced; however, the total radiated yield (including K-shell component) is comparable with those of the wire arrays as shown in Fig. 18. These observations indicate that a similar amount of energy was deposited into the plasma, in all cases. With these caveats in mind, it is clearly the case that the single wire did not achieve significant bulk K-shell ionization. This is probably due to the fact that the Ohmic heating cannot overcome the large radiation rates when the plasma is in the L shell. This is illustrated by Fig. 19, which shows a plot of the radiation power from a 3-mm-diam, 200-μg/cm aluminum plasma as a function of temperature. Also shown are the estimated Ohmic heating powers based on Spitzer resistivity as functions of temperature, in the range 200–2000 eV. Curves are drawn using ten times classical transverse Spitzer resistivity and 100 times Spitzer resistivity. The multiplication factors are arbitrary and are not based on any self-consistent physics.

Since in the L-shell phase at a temperature around 200 eV, the Ohmic heating is outweighed by the radiation

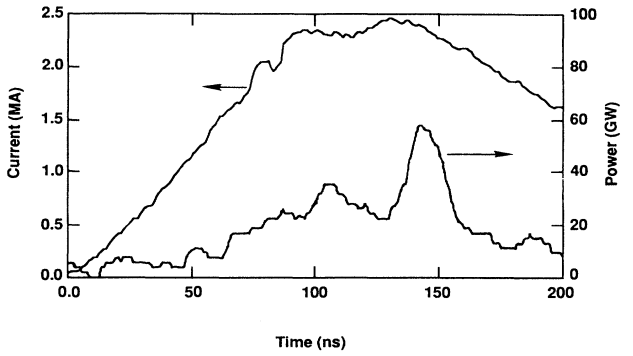

FIG. 17. Load current and K-shell x-ray power for a 100-μm-diam single aluminum wire. The emission powers are low and the spiked structure is indicative of hot spots.

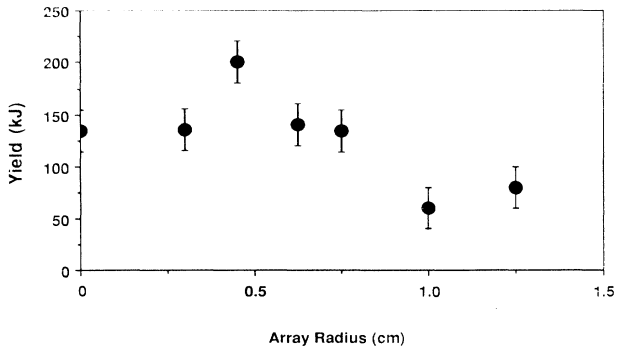

FIG. 18. Measured total radiated yield vs initial array radius, including the single wire. The total radiated yield for the single wire is comparable to those of the arrays.

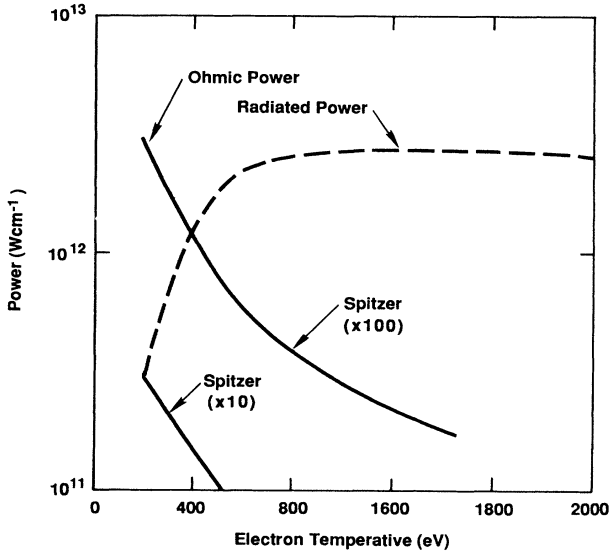

FIG. 19. Radiated power and Ohmic heating for a 3-mm-diam aluminum plasma vs the electron temperature. The Ohmic heating assumes the classical Spitzer formulation, but it is increased arbitrarily by 10 and 100.

losses, the plasma electron temperature is probably clamped. Even at ten times classical Spitzer resistivity, these radiation rates dominate. If the electron temperature cannot rise because L-shell radiation losses equal (or exceed) the Ohmic heating, the overall plasma can never achieve K-shell ionization. Why the plasma does not undergo a radiative collapse is unclear and should be the subject of future research; however, we can conclude that a single wire, when driven by a 100-ns current pulse, cannot be heated Ohmically or otherwise, fast enough to achieve K-shell ionization. The localized heating mechanisms, which form the hot spots and produce the local K-shell ionization, are still speculative.

Based on the experimental data, it would appear that an implosion phase with $\eta > 1$ is required to achieve more uniform K-shell ionization. The instantaneous power deposition due to the thermalization of the kinetic energy is high; assuming the collapse kinetic energy is 15 kJ/cm (see Table VI) and this energy takes between a maximum of 15 ns and a minimum of 5 ns to thermalize, then the power deposition is in the range 1–3 TW/cm. These numbers are, of course, significantly less than the 10-TW/cm instantaneous power levels which are predicted by the calculations in Ref. [10]. Referring back to Fig. 19, the 1–3-TW/cm power levels certainly exceed the radiation rates for temperatures around 200 eV. Under these circumstances, at thermalization, the plasma would be rapidly ionized through the L-shell to the K-shell. Thus the single-wire data and the power estimates seem to support the "ignition" concept.

VI. SUMMARY AND CONCLUSIONS

The purpose of this paper is to evaluate the role of the implosion kinetic energy in prescribing the K-shell x-ray yield from aluminum-wire-array Z-pinch implosions. We make this evaluation both by varying the initial array radius (while keeping $m_0 r^2$ approximately constant) and by comparing experiments with 1D laminar MHD calculations. We find that the kinetic energy is necessary to guarantee that the imploding plasma is ionized into the K shell. Quantitatively, this can be expressed by saying that the dimensionless kinetic energy per ion η must be made to exceed 1. On the other hand, in the face of the experimental data, we have reappraised the assumption that this kinetic energy is the sole energy source for the K-shell (and total) radiations. Conservative nonturbulent MHD calculations dictate that the maximum conversion efficiency of kinetic energy to K-shell radiation is 30–40% near η equal to 1. Moreover, the calculations predict an almost constant K-shell yield for the 0.625- to the 1.0-cm-radius implosions because they are in the I^2 regime. This is not born out by the experiment; we actually observe an optimum x-ray yield for the 0.625-cm implosion, which is more than twice the predicted value.

Additional heating mechanisms have to be invoked to explain the differences between the measured and predicted yields. Straightforward classical Spitzer resistivity cannot account for enough Ohmic heating to be the missing energy source. However, if the plasma exhibits anomalous resistivity, possibly due to turbulence, then Ohmic heating may be the answer. It is likely, however, that the additional heating will depend on the magnitude of the current flowing through the pinch at thermalization and on the plasma parameters such as diameter, temperature, density, and mass assembled.

The implication of these observations on optimizing the x-ray yield on imploding Z pinches is apparent. On a given generator, the implosion time may be made equal to the time to peak current because this ensures the maximum current flow through the pinch and the maximum kinetic-energy generation. The initial radius should apparently then be chosen to give η as close to 1 as possible, thus maximizing the mass. Following this algorithm, should ensure that the x-ray yield is maximized, if additional heating is strong. Future experiments should investigate the initial expansion of the wire arrays or another approach may be to compare gas puff implosions with 1D laminar calculations because gas puffs resemble better the initial assumptions of 1D calculations, as regards mass distribution. The influence of 2D effects, turbulence, anomalous transport coefficients may also modify the 1D calculations to better approximate the experimental plasma behavior and this should give further insight into the additional heating mechanisms that appear to supplement the thermalization of the kinetic energy.

ACKNOWLEDGMENTS

We would like to acknowledge beneficial discussions with John Giuliani, Ted Cochran, Dave Mosher of NRL; Mahadevan Kirshnan of SRL; and Rick Spielman of SNLA. Norm Knobel and the Double-EAGLE crew are thanked for their technical assistance.

*Present address: Berkeley Research Associates, Springfield, Virginia.

[1] C. Stallings, K. Nielsen, and R. Schneider, Appl. Phys. Lett. **29**, 404 (1976).
[2] J. Katzenstein, J. Appl. Phys. **52**, 767 (1981).
[3] M. Gersten, W. Clark, J. E. Rauch, G. M. Wilkinson, J. Katzenstein, R. D. Richardson, J. Davis, D. Duston, J. P. Apruzese, and R. Clark, Phys. Rev. A **33**, 477 (1986).
[4] C. Deeney, T. Nash, P. D. LePell, K. Childers, M. Krishnan, K. G. Whitney, and J. W. Thornhill, J. Quant. Spectrosc. Radiat. Transfer **44**, 457 (1990).
[5] R. B. Spielman, D. L. Hanson, M. A. Palmer, M. K. Matzen, T. W. Hussey, and J. M. Peek, J. Appl. Phys. **57**, 883 (1985).
[6] W. Clark, R. Richardson, J. Brannon, M. Wilkinson, and J. Katzenstein, J. Appl. Phys. **53**, 5552 (1982).
[7] F. C. Young, S. J. Stephanakis, V. E. Scherrer, B. L. Welch, G. Mehlman, P. G. Burkhalter, and J. P. Apruzese, Appl. Phys. Lett. **50**, 1053 (1987).
[8] S. Wong, C. Gilman, P. Sincerny, and T. Young (unpublished).
[9] D. Mosher, Naval Research Laboratory Memo Report No. 3687, 1978 (unpublished).
[10] K. G. Whitney, J. W. Thornhill, J. P. Apruzese, and J. Davis, J. Appl. Phys. **67**, 1725 (1990).
[11] S. J. Stephanakis *et al.*, Naval Research Laboratory Plasma Technology Technical Note No. 85-51, 1985 (unpublished).
[12] T. Nash, C. Deeney, M. Krishnan, R. R. Prasad, P. D. LePell, and L. Warren, J. Quant. Spectrosc. Radiat. Transfer **44**, 485 (1990).
[13] M. C. Coulter, K. G. Whitney, and J. W. Thornhill, J. Quant. Spectrosc. Radiat. Transfer **44**, 443 (1990).
[14] P. Sincerny, D. Strachan, G. Frazier, C. Gilman, H. Halava, S. Wong, J. Bannister, T. DaSilva, S. K. Lam, P. D. LePell, J. Levine, R. Rodenburg, and T. Sheridan (unpublished).
[15] R. H. Day, P. Lee, E. B. Saloman, and D. J. Nagel, J. Appl. Phys. **52**, 6965 (1981).
[16] F. C. Young, S. J. Stephanakis, and V. E. Scherrer, Rev. Sci. Instrum. **57**, 2714 (1986).
[17] P. Burkhalter, J. Davis, J. E. Rauch, W. Clark, G. Dahlbacka, and R. E. Schneider, J. Appl. Phys. **50**, 705 (1979).
[18] J. C. Riordan, J. S. Pearlman, M. Gersten, and J. E. Rauch, in *Low-Energy X-Ray Diagnostics, 1981, Monterey, CA,* Proceedings of Topical Conference on Low Energy X-Ray Diagnostics, AIP Conf. Proc. No. 75, edited by D. T. Attwood and B. Henke (AIP, New York, 1981), p. 35.
[19] D. Mosher, S. J. Stephanakis, I. M. Vitkovitsky, C. M. Dozier, L. S. Levine, and D. J. Nagel, Appl. Phys. Lett. **23**, 429 (1973).
[20] L. E. Aranchuk, S. L. Bogolyubski, G. S. Volkov, V. D. Korolev, Yu. V. Koba, V. I. Liksonov, A. A. Lukin, L. B. Nikandrov, O. V. Tel'Kovskaya, M. V. Tulupov, A. S. Cherenko, V. Ya. Tsarfin, and V. V. Yan'kov, Sov. J. Plasma Phys. **12**, 765 (1986).
[21] A. Ya Faenov, J. Phys. D **18**, 1347 (1985).
[22] J. Giuliani, J. E. Rogerson, C. Deeney, T. Nash, R. R. Prasad, and M. Krishnan, J. Quant. Spectrosc. Radiat. Transfer **44**, 471 (1990).